



HAL
open science

The geometric and thermohydraulic characterization of ceramic foams: An analytical approach

Prashant Kumar, Frederic Topin

► To cite this version:

Prashant Kumar, Frederic Topin. The geometric and thermohydraulic characterization of ceramic foams: An analytical approach. *Acta Materialia*, 2014, 75, pp.273-286. 10.1016/j.actamat.2014.04.061 . hal-01459370

HAL Id: hal-01459370

<https://hal.science/hal-01459370>

Submitted on 10 Feb 2023

HAL is a multi-disciplinary open access archive for the deposit and dissemination of scientific research documents, whether they are published or not. The documents may come from teaching and research institutions in France or abroad, or from public or private research centers.

L'archive ouverte pluridisciplinaire **HAL**, est destinée au dépôt et à la diffusion de documents scientifiques de niveau recherche, publiés ou non, émanant des établissements d'enseignement et de recherche français ou étrangers, des laboratoires publics ou privés.

The geometric and thermohydraulic characterization of ceramic foams: An analytical approach

Prashant Kumar*, Frederic Topin

IUSTI, CNRS UMR 7343, Aix-Marseille University, Marseille, France

Abstract

Knowledge of the thermohydraulic properties of industrial components is often necessary for planning and designing chemical engineering processes. The thermohydraulic behavior of open-cell foams depends on their microscopic structure. Based on the tetrakaidecahedron geometry and different strut morphologies of the ceramic foams, we have derived a generalized analytical model that encompasses all geometrical parameters precisely. A special treatment is developed to take the hollow nature of ceramic foam struts into account. Various relationships between different geometrical parameters and porosities are presented. As strut geometries substantially affect flow characteristics, correlations have been developed to determine the hydraulic diameter for ceramic foams using geometric parameters from measured pressure drop data. Two analytical models are derived in order to predict intrinsic solid phase conductivity, λ_s , and effective thermal conductivity, λ_{eff} , simultaneously. A modified correlation term, F , is introduced in the analytical resistor model to take into account the thermal conductivities of constituent phases and a modified Lemlich model is derived. The analytical results are compared with the experimental data reported in the literature and an excellent agreement is observed.

1. Introduction

Open-cell foam (ceramic or metallic) is a cellular material defined by solid material surrounded by a three-dimensional network of voids. As a lightweight porous material, open-cell foam possesses a high strength and stiffness relative to its weight, making it an attractive option for a variety of applications. In comparison with packed beds of spheres, open-cell foams have higher specific surface area, leading to higher external mass transfer rates. They are also highly porous, which results in low pressure drop. Their specific shape enhances the mixing and improves heat transfer [1–5].

For the application of foam structures as catalyst supports in chemical engineering, reticulated ceramic foams have many attractive features [6,7]. For the planning and designing of numerous chemical engineering processes, precise knowledge of geometrical characteristics, specific surface area and pressure-drop properties is extremely important [7–16]. The relationship between geometrical parameters and thermal properties such as the effective thermal conductivity is critical for conductive heat transfer in foams of highly porous cellular materials, mainly metal foams [17–21]. The continuous strut network enables good heat conductivity, and the void structure allows for pronounced heat transfer through radiation at elevated temperatures.

There are various methodologies for manufacturing ceramic foams. One method involves direct foaming (gel casting) [22], giving solid struts without internal voids.

Nomenclature

Latin symbols

a_c	Specific surface area, m^{-1}
$A]_D$	Ergun parameter, dimensionless [15], Eq.3
$B]_D$	Ergun parameter, dimensionless [15], Eq.3
$A]_E$	Ergun parameter, dimensionless, Eq. 1
$B]_E$	Ergun parameter, dimensionless, Eq. 1
C	Correction factor, dimensionless
d_{cell}	Cell diameter, m
d_h	hydraulic diameter, m
$d_{h]D}$	hydraulic diameter, m [15], Eq.3
d_p	Pore diameter, m
D_p	Particle diameter, m
d_s	Strut diameter, m
d_w	Window diameter, m
F	Constant, dimensionless
K_1	Permeability coefficient of viscous term, m^2
K_2	Permeability coefficient of inertial term, m
L	Node length, m
L_s	Strut length, m
ΔL	Length of the foam, m
n	Constant, dimensionless
N	Void length, m
ΔP	Pressure drop, Pa
R	Strut Radius, m
Re	Reynolds number, dimensionless
S	Constant, dimensionless
V_s	Solid volume of foam, m^3

V_T Total volume of cubic cell, m^3

Greek symbols

ε_n	Nominal porosity, dimensionless
ε_t	Total porosity, dimensionless
ε_0	Open porosity, dimensionless
ε_s	Strut porosity, dimensionless
Ω	Constant, dimensionless
α	Constant, dimensionless
β	Constant, dimensionless
χ	Constant, dimensionless
Λ	Constant, dimensionless
μ	Dynamic viscosity, kg/m/s
ρ	Density of fluid, kg/m^3
λ_s	Intrinsic solid phase conductivity, W/mK
λ_f	Fluid phase conductivity, W/mK
λ_{eff}	Effective thermal conductivity, W/mK
$\lambda_{parallel}$	Parallel thermal conductivity, W/mK
λ_{series}	Series thermal conductivity, W/mK
ζ	Numerical value, Dimensionless
Π	Numerical value, Dimensionless
ψ	Constant, dimensionless

Abbreviations

CT	Computed tomography
MRI	Magnetic resonance imaging
PPI	Pores per inch

The other commonly employed method is a replication technique that results in foams featuring hollow struts (internal voids in the struts) which are not normally accessible to fluid flow [23]. The foam matrices can be described by their morphological parameters, namely cell and window diameter, strut thickness and porosity [8,12].

Due to the unavailability of resources to measure the specific surface area of ceramic foams, Richardson et al. [8] used the relationships of Gibson and Ashby [24] to derive the specific surface area (a_c) for the pentagonal dodecahedron geometrical model. Similarly, Buciuman et al. [25] developed the expression for calculating the specific surface area of ceramic foams using the approach of Gibson and Ashby [24]. Lacroix et al. [11] used the cubic cell model (considering solid struts) to develop the correlation for the specific surface area, using the open porosity (ε_0) of the foam structure and the strut thickness (d_s). The expressions derived by these authors [8,11,25] induce many discrepancies in determining specific surface area precisely. Moreover, these expressions are based on only two geometrical parameters and do not attain the same results because of low-accuracy measurements or ill-defined geometrical quantities.

Recently, with the advancement in measurement techniques and the evolution of new methodologies, a few

authors [13,26] have used magnetic resonance imaging (MRI) to measure the specific surface area of ceramic foams. These authors investigated ceramic alumina foams using MRI. X-ray computed tomography (CT) has been applied by different authors to characterize the morphological parameters of foam structures [27].

Incera Garrido et al. [13] have reported that the cubic model proposed by Lacroix et al. [11] results in a stronger overprediction of the surface area than the tetrakaidecahedron model. Grosse et al. [26] used the Weaire–Phelan structure to model their foams. They derived the correlation using nominal porosity (ε_n) and later used an empirical fitting procedure to redefine the coefficient using open porosity and obtained the semi-empirical correlation which gave close agreement with their experimental data. Inayat et al. [16] have proposed empirical correlations (for different strut shapes, namely triangular, circular and concave triangular) using the geometrical relationships of Richardson et al. [8] with open porosity, window and strut diameter. Their correlation is in good agreement with experimental specific surface area. Inayat et al. [16] argued that the tetrakaidecahedra unit cell should be used, because this is the most consistent with the observed properties and derived geometric relationships for the unit cell (see also Gibson and Ashby [24]). Importantly, the regular

dodecahedron is not a space-filling shape, and thus may not be as appropriate as the periodic unit cell as discussed in Refs. [16,28,29]. Moreover, some of the correlations are derived using empirical fitting on a small set of samples, and thus cannot be directly applied to characterize ceramic foams.

It is known that the pressure drop from one-dimensional flow through a porous medium is given by the sum of two terms: a viscous term and an inertia term and is well described by the Forchheimer equation as:

$$\frac{\Delta P}{\Delta L} = \frac{\mu}{K_1} V + \frac{\rho}{K_2} V^2. \quad (1)$$

The flow properties, K_1 and K_2 , are deduced by second-order polynomial fitting from experiments. It is common practice to relate K_1 and K_2 to the geometrical properties of foams (e.g. d_p and ε_o). Knowledge of the pressure drop induced by foam matrices is essential for the successful design and operation of high-performance industrial systems. During the last decade, numerous experiments and analytical models on single-phase flow in solid foams have been established (see data gathered by Mahjoob and Vafai [30], Bonnet et al. [31] and Edouard et al. [32]). Many authors have adopted an Ergun-like approach [33] to derive correlations by fitting their experimental data according to the following equation:

$$\frac{\Delta P}{\Delta L} = A]_E \frac{(1 - \varepsilon_o)^2}{\varepsilon_o^3} a_c^2 \mu V + B]_E \frac{(1 - \varepsilon_o)}{\varepsilon_o^3} a_c \rho V^2, \quad (2)$$

where $A]_E$ and $B]_E$ are parameters that are dependent on the foam geometry.

Many authors (e.g. [8,9,11]) usually replaced a_c with an evaluation-based characteristic size, L_c (usually $a_c \approx \text{constant}/L_c$). This L_c is chosen either as D_p or d_p or d_s (with various definitions) and these authors adapted the analogy between solid foam and spherical particles with the same specific surface area per unit volume and the same porosity even if foams do not possess the same geometry, which leads to $D_p = 1.5d_s$ or $D_p = 6(1 - \varepsilon_o)/a_c$.

Literature review has suggested that the pressure drop of foams (metallic or ceramic) is dependent not only on one characteristic dimension (e.g. D_p) and porosity (ε_o) but also on other geometrical characteristics of the solid topology. Using direct numerical simulations at pore scale, Hugo and Topin [34] observed that at a constant pore size, flow properties K_1 and K_2 could vary by about one order of magnitude (error of $\sim 100\%$). They concluded that the traditional form of the Ergun-like approach is not sufficient to describe the pressure drop and thus new geometrical parameters should be added.

One of the major problems in calculating the pressure drop in the foams by using the Ergun-like approach is to define structural properties of porous media reliably in order to replace the particle diameter (D_p). Typical values of $A]_E$ and $B]_E$ resulting from these approaches that were used in these correlations range from 100 to 865 and 0.65

to 2.65, respectively (see data gathered by Mahjoob and Vafai [30]). A few of the most significant reasons for such a wide dispersion in the values of Ergun parameters are the assumption of oversimplified foam geometry, the analogy between the foam and spherical particles, and the unavailability of full sets of measured geometrical properties. Many of the apparent discrepancies are merely due to the choice of characteristic length or its definition.

In order to derive a pressure drop correlation, the authors use various definitions of porosity (total or open porosity) as well as the porosity functions in viscous and inertia terms (e.g. [15]). Similarly, hydraulic diameter ($d_h = 4\varepsilon_o/a_c$) is one of the characteristic dimensions that could be used to determine the Reynolds number correctly and should be related to the friction factor [31].

Dietrich et al. [15] proposed using the hydraulic diameter, which takes into consideration the total porosity due to an absence of a full set of open porosity of Mullite and OBSiC foam samples. They used a slightly different formula than the Ergun-like approach, given by following expression as:

$$\frac{\Delta P}{\Delta L} = A]_D \frac{1}{\varepsilon_t \cdot d_h]_D^2} \mu V + B]_D \frac{1}{\varepsilon_t^2 \cdot d_h]_D} \rho V^2 \text{ with } d_h]_D = \frac{4\varepsilon_t}{a_c}. \quad (3)$$

They also proposed the constant values of parameters, $A]_D$ and $B]_D$ as 110 and 1.45, respectively.

Several authors (e.g. see data gathered by Mahjoob and Vafai [30], Edouard et al. [32]) have studied the pressure-drop correlations and concluded that no universally applicable correlation for single-phase pressure drop of foams exists so far. On the other hand, Dietrich [35] showed that their correlation could predict the experimental pressure drop from open literature for both ceramic and metal foams with the majority of the data points lying between $\pm 40\%$ for a high porosity range (0.85–0.95). For a known strut shape (e.g. triangular strut shape) and small range of high porosity, it could be possible to obtain the constant numerical values of Ergun parameters.

Commercially available foams of different materials presented in the literature lie in a small porosity range ($\varepsilon_o \approx 0.90 \pm 5\%$). Usually, at higher porosity (0.85–0.95) and for a given pore size, the inertia coefficient K_2 does not vary much with respect to different strut shapes (circular, triangular, convex or concave triangular). However, in the case of low porosity (0.60–0.85), the inertia coefficient K_2 varies tremendously and depends strongly on strut shape. With respect to strut shapes of either ceramic or metal foams, Ergun parameters cannot have a constant value but should be dependent on foam geometry.

In the literature, however, several authors agree that $A]_E$ and $B]_E$ are not constant, but rather depend upon the properties of the medium [7,8,34,36]. Inayat et al. [36] have developed a dimensionless correlation for parameters $A]_E$ and $B]_E$ that depends upon the window diameter, strut diameter and open porosity of the foams. They argued that the numerical values appearing in their correlation are

geometric constants of foam geometry. They correlated Ergun parameters only with open porosity. Their correlation showed that the Ergun equation with fixed parameters or unchanged coefficients ($A]_E$ and $B]_E$) cannot be applied to predict pressure drop for foam structures for a wider range of high porosity (0.7–0.95).

There are several kinds of empirical correlations in the literature that determine effective thermal conductivity (λ_{eff}) in a local thermal equilibrium condition (LTE). Effective thermal conductivity is the thermal conductivity of an equivalent homogeneous medium with the same thermal behavior as the original one [37]. One group of effective thermal conductivity studies focuses on the asymptotic bound approach while the others deal with the microstructural approach.

Lemlich [38] has developed an analogy to predict the electrical conductivity of polyhedral liquid foam of high porosity and this is given by the following equation:

$$\lambda_{eff} = \frac{1}{3}\lambda_s(1 - \varepsilon_t). \quad (4)$$

The limitation of using the Lemlich model [38] is that it does not predict an approximate value of λ_{eff} when water is used as the fluid medium, but works well with air as the fluid medium. In fact, this model takes only heat conduction in the solid phase into account. When the fluid phase conductivity is of the same order of magnitude of solid-phase conductivity, this model is no longer valid because of significant heat exchange between foam ligament and interstitial fluid and therefore Eq. (4) is not appropriate in determining λ_{eff} .

In the literature, many authors [39–45] have rigorously used the solid-phase thermal conductivity of the parent material (e.g. pure Al/Al 6101 T alloy) to predict the effective thermal conductivity using empirical correlations of the asymptotic approach. Manufacturing processes greatly impact the solid-phase thermal conductivity of the parent material when transformed into foams. As various commercially available foams employ different manufacturing techniques; there are significant differences in the intrinsic solid-phase thermal conductivity of foams compared to the same parent material one. None of these authors have measured the intrinsic value or actual value of the solid-phase thermal conductivity of foam materials.

In general, the intrinsic solid-phase thermal conductivity of the strut or foam is unknown when experiments are performed to determine the effective thermal conductivity. Dietrich et al. [46] have measured the intrinsic solid-phase conductivity of their ceramic foam samples. They have also derived the effective thermal conductivity correlation using the asymptotic approach and related it to porosity and to two experimental fitting parameters.

Using 3-D numerical simulations, Hugo [47] showed that the ratio of conductivity between phases impacts on the thermal conductivity under the condition of local thermal equilibrium. When the fluid-phase conductivity has the same order as the solid phase, the fluid phase starts to play

an important role in determining the effective thermal conductivity. In this case, the correlations given by several authors [39–45] will not hold and actually induce a large error, as shown in the works of Dietrich et al. [46]. Hugo [47] has shown that porosity alone is not the parameter determining the effective thermal conductivity, which must be related to other geometrical parameters of foam matrix. Moreover, all these correlations do not take into account the real morphology of the foam, but assume an idealized periodic pattern.

In this work, we develop a generalized model for ceramic foams of porosity $\varepsilon_t \leq 0.90$ (based on the tetrakaidecahedron geometry) for the theoretical estimation of the specific surface area of ceramic foams applicable for different foam materials, porosities and pore densities, and validate this model experimentally. Our methodology can be extended to any type of foam (metallic or ceramic; with or without hollow struts) and for porosity $0.65 \leq \varepsilon_t \leq 0.95$. We have mainly focused on the constant cross-section of the ligament along its axis.

We also propose a combination of dimensionless geometrical parameters as a correction factor to the approach put forth by Dietrich et al. [15] that predicts Ergun parameters analytically. We show the importance of this dimensionless geometrical parameter and its influence on flow characteristics.

To the best of our knowledge, no study has identified the need for an effective thermal conductivity model that encompasses geometrical parameters of foams and intrinsic solid to fluid thermal conductivity ratios. We use the solid conductivity of the parent material to assign the solid conductivity of material by nature (e.g. Al). We use the intrinsic thermal conductivity of the material that constitutes the phase or form of the foam (e.g. the thermal conductivity of the strut of Al), which usually differs from that of the parent material.

Two models have been presented in this paper, namely the resistor model and the modified Lemlich model that includes both unknowns, λ_s and λ_{eff} . They can be used in either way: when λ_s is known to determine λ_{eff} or vice versa. These models can also be used to solve a problem simultaneously as a system of two linear equations where both λ_s and λ_{eff} are unknowns but the fluid-phase thermal conductivity is known.

2. Geometrical modeling

2.1. Parametric characterization of geometry

Depending on the manufacturing processes (see Section 1), most of the commercially available ceramic foams exhibit hollow struts. A typical hollow strut is shown in Fig. 1. Based on tetrakaidecahedron geometry inside a cubic cell (see Fig. 2) of the circular nature of strut for total porosity range $0.65 \leq \varepsilon_t \leq 0.90$, an analytical model has been derived that covers the strut for both open and total porosity. Fig. 1 (right) shows the dimension of the circular

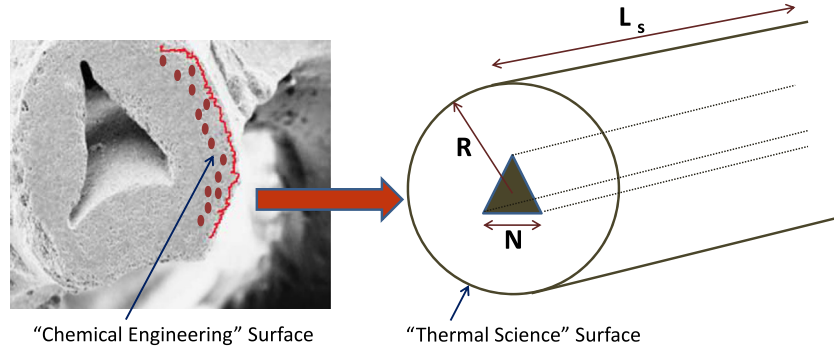


Fig. 1. Left: presentation of a typical hollow ceramic strut. Right: a detailed circular strut cross-section with an equilateral triangular void inside the strut. The dimensions of strut (strut radius, R) and void cross-section (void length, N) are clearly highlighted.

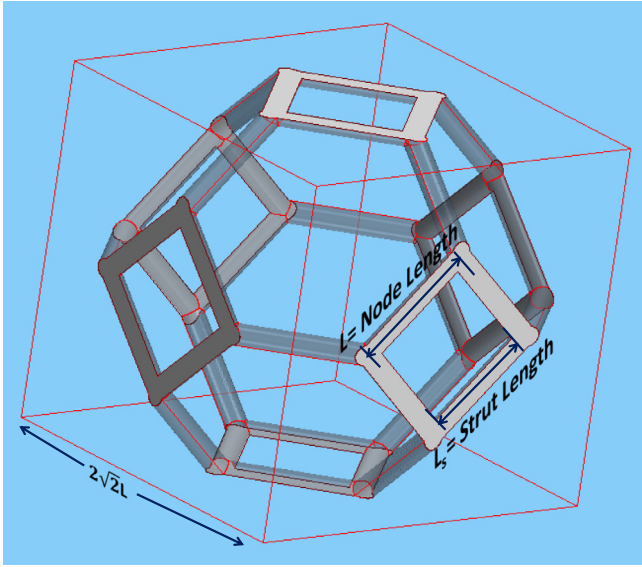


Fig. 2. A tetrakaidecahedron model inside a cube. Node length L (center-to-center distance of a node connection), strut length L_s and cubic unit cell length $2\sqrt{2}L$ are clearly presented. The analytical model is based on the above unit cell having a triangular void in the struts.

strut radius, R , and an approximated equilateral triangular void of side length, N .

In order to provide an approximate analytical solution, L_s has been defined as the strut length (without considering nodes) and L as the distance between two nodes (or length of solid truncated octahedron edge) as shown in Fig. 2.

Strut porosity due to voids inside the strut is calculated as:

$$\varepsilon_s = \frac{V_{void}}{V_{strut}} = \frac{\sqrt{3}/4N^2L_s}{\pi R^2L_s}. \quad (5)$$

Eq. (5) can be rewritten as:

$$N = \Omega R, \quad (6)$$

where $\Omega = \sqrt{4\pi\varepsilon_s/\sqrt{3}}$.

We chose to base our node volume on the calculation given by Kanaun and Tkachenko [48]. The volume of the node at the junction of four struts is given (see Fig. 3) as:

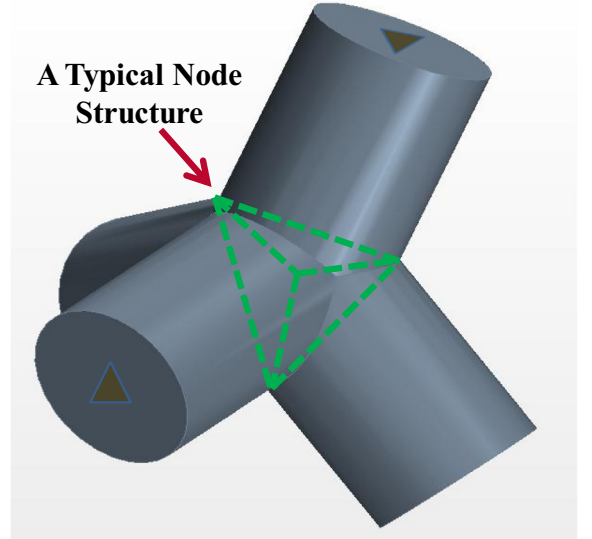


Fig. 3. A typical node of foam structure. We have shown the four faces of a pyramid which is taken into consideration in calculating the volume of the node. The face of the nodes changes with the strut shape. We have shown four struts of circular shape at the node which is approximated as a triangular pyramid.

$$V_{node} = \frac{4}{3} \left(\pi R^3 - \frac{\sqrt{3}}{4} N^3 \right) = \frac{4}{3} \pi R^3 (1 - \Omega \varepsilon_s). \quad (7)$$

The volume of the ligament is given as:

$$V_{ligament} = \pi R^2 L_s - \frac{\sqrt{3}}{4} N^2 L_s = \pi R^2 L_s (1 - \varepsilon_s). \quad (8)$$

At the node junction, we can approximate the node by using a geometrical interpretation as shown in Fig. 3:

$$1.6R + L_s = L. \quad (9)$$

In dimensionless form, we can rewrite Eq. (9) as:

$$1.6\alpha + \beta = 1, \quad (10)$$

where $\alpha = \frac{R}{L}$ and $\beta = \frac{L_s}{L}$.

In a truncated octahedron structure (see Fig. 2), there are 36 ligaments and 24 nodes, but only one-third of the volume of both ligaments and nodes are included in the

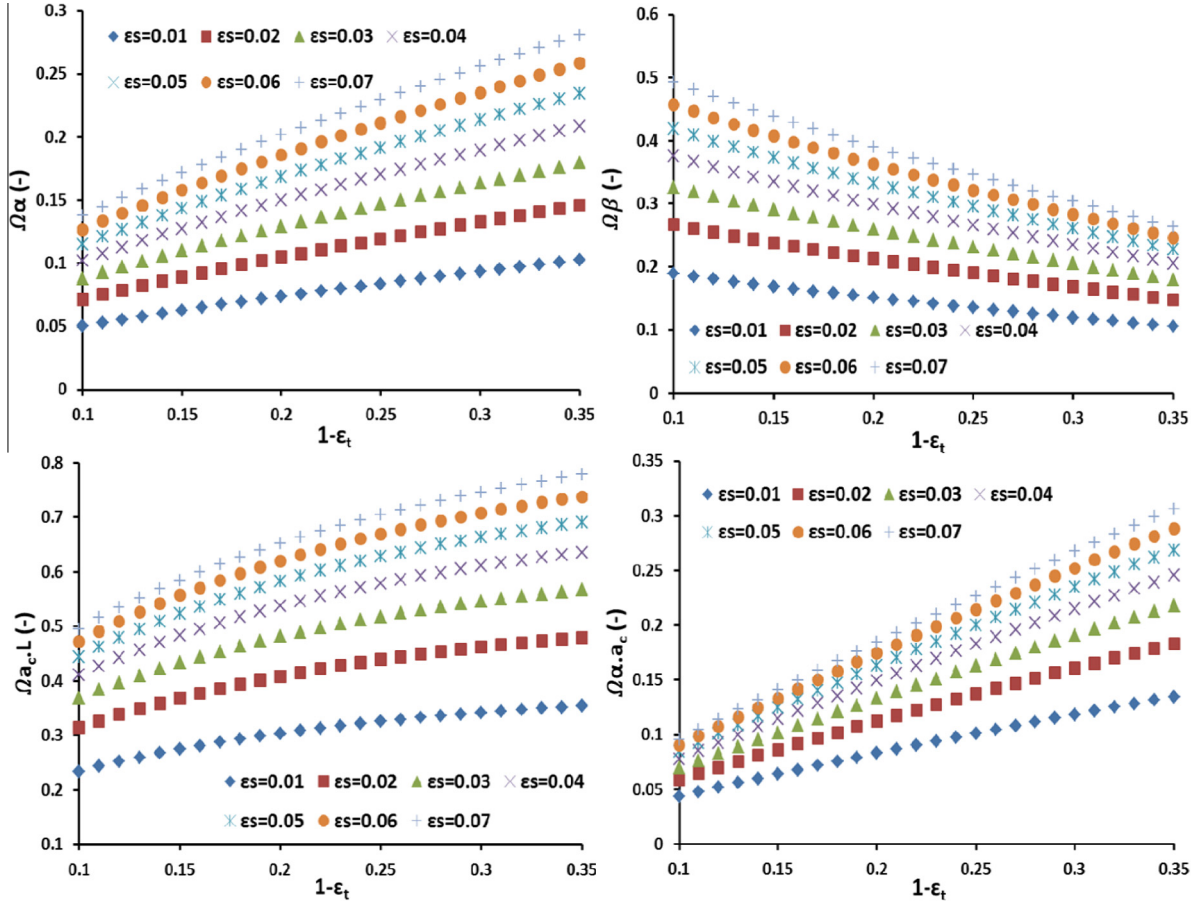


Fig. 4. Plot of non-dimensional geometrical parameters vs. $1 - \varepsilon_t$ for different strut porosities, ε_s . Top left: $\Omega\alpha$ function of hollow strut and strut diameter. Top right: $\Omega\beta$ function of hollow strut and strut length. Bottom left: $\Omega a_c L$ function of hollow strut, specific surface area and node length. Bottom right: $\Omega\alpha a_c$ function of hollow strut, strut diameter and specific surface area. Geometrical characteristics of any foam can be derived by using a combination of the curves presented above. Also, one can tailor one's own foams accordingly for specific engineering applications.

unit periodic cell. For periodic cellular foam in a unit cell, the total solid volume (V_s), total truncated volume ($V_T = 8\sqrt{2}L^3$) and total porosity (ε_t) are related as:

$$\begin{aligned} \varepsilon_t &= \frac{1 - \frac{1}{3}(36V_{ligament} + 24V_{node})}{V_T} \\ &= \frac{1 - \frac{1}{3}(36\pi R^2 L_s(1 - \varepsilon_s) + 24 \cdot \frac{4}{3}\pi R^3(1 - \Omega\varepsilon_s))}{8\sqrt{2}L^3}. \end{aligned} \quad (11)$$

In dimensionless form, we can rewrite Eq. (11) as:

$$12\pi\alpha^2\beta(1 - \varepsilon_s) + \frac{32}{3}\pi\alpha^3(1 - \Omega\varepsilon_s) = 8\sqrt{2}(1 - \varepsilon_t). \quad (12)$$

Eq. (12) gives a generic relation of total porosity as a function of geometrical parameters. Note that α is the ratio of strut radius to node length, whereas β is the ratio of strut length to node length. We could combine Eqs. (10) and (12) to find approximate values of α and β as functions of ε_t . This approach can be used to determine all the geometrical properties if the full set of geometrical parameters is not known.

Strut porosity (ε_s), strut radius (R) and strut length (L_s) are interrelated. In order to see the effects of each parameter on the geometrical characteristics, different values of

$\Omega\alpha$ and $\Omega\beta$ have been plotted against different porosities (ε_t) and are found to follow power and exponential laws, respectively, as shown in Fig. 4 (top left and top right), and can be expressed as:

$$\Omega\alpha = \chi_1(1 - \varepsilon_t)^{\Lambda_1}, \quad (13)$$

$$\Omega\beta = \chi_2 \exp[-\Lambda_2(1 - \varepsilon_t)], \quad (14)$$

where χ and Λ are parameters that depend only on void shape and are functions of total porosity.

For instance, for a given hollow strut porosity and total porosity, one can easily quantify the strut radius and strut length. Moreover, depending upon the desired output quantity for industrial applications, one could tailor one's own foam characteristics using Eqs. (13) and (14) and Fig. 4 (top left and top right).

It is clearly evident from Fig. 2 that there are 12 full ligaments and 24 half ligaments in a unit cell. Also, at the node junction, there are two half nodes and one quarter node. As it is far more convenient to calculate the specific surface area using a cubic unit cell, the foam structure has been considered in a cubic cell of volume V_c . The specific surface area, a_c , can be written as:

Table 1

Properties of alumina, Mullite, OBSiC and SSiC foams of different porosities and pore sizes. Experimental and analytical data are presented.

Authors	Material	Experimental data							Analytical data		
		d_w	d_s	ε_n	ε_t	ε_o	a_c (MRI)	a_c [15]	ε_o	ε_s	a_c
Garrido et al. [13]	Alumina	1.069	0.46	0.75	0.777	0.719	1290			0.058	1176
		1.933	0.835	0.80	0.818	0.772	675			0.046	678
		1.192	0.418	0.80	0.804	0.751	1187			0.053	1262
		0.871	0.319	0.80	0.816	0.766	1438			0.05	1520
		0.666	0.201	0.80	0.813	0.761	1884			0.052	2043
		2.252	0.88	0.85	0.852	0.812	629			0.04	589
		1.131	0.451	0.85	0.858	0.814	1109			0.044	1031
		0.861	0.33	0.85	0.852	0.807	1422			0.045	1353
Grosse et al. [26]		0.687	0.206	0.85	0.848	0.801	1816			0.047	2048
		1.974	1.001	0.75	0.75	0.688	639			0.062	646
		1.070	0.651	0.75	0.736	0.719	1260			0.017	1176
		1.796	0.944	0.80	0.794	0.773	664			0.021	641
		0.955	0.509	0.80	0.814	0.745	1204			0.069	1107
		0.847	0.391	0.80	0.816	0.754	1474			0.062	1246
		0.781	0.276	0.80	0.801	0.763	1884			0.038	2012
		1.952	0.809	0.85	0.848	0.812	629			0.036	593
		1.137	0.544	0.85	0.853	0.813	1109			0.04	998
		0.860	0.273	0.85	0.87	0.793	1520			0.077	1246
Dietrich et al. [15]	Al ₂ O ₃	0.651	0.217	0.85	0.843	0.783	1816			0.06	1943
		1.529	0.651	0.75	0.754	0.69	1090			0.064	1155
		2.253	0.967	0.80	0.808	0.765	664			0.043	612
		1.091	0.476	0.80	0.802	0.748	1204			0.054	1290
		0.884	0.391	0.80	0.806	0.752	1402			0.054	1542
		0.625	0.195	0.80	0.809	0.757	1884			0.052	1801
	Mullite	1.464	0.544	0.85	0.854	0.811	1109			0.043	991
		1.348	0.612	0.75	0.736	–	–	1035	0.695	0.041	1160
		2.111	0.895	0.80	0.785	–	–	638	0.741	0.044	654
		1.405	0.545	0.80	0.789	0.741	1291			0.048	1187
		1.127	0.533	0.80	0.793	0.748	1395			0.045	1190
		0.685	0.293	0.80	0.797	0.744	2126			0.053	2143
	OBSiC	1.522	0.51	0.85	0.834	–	–	879	0.787	0.047	846
		1.361	0.896	0.75	0.742	–	–	899	0.701	0.041	858
		2.257	1.063	0.80	0.791	–	–	578	0.747	0.044	601
		1.489	0.719	0.80	0.791	–	–	869	0.747	0.044	889
		1.107	0.544	0.80	0.791	–	–	1162	0.747	0.044	1175
		0.715	0.275	0.80	0.786	–	–	1938	0.742	0.044	2374
Inayat et al. [16]	SSiC	1.467	0.622	0.85	0.845	–	–	855	0.798	0.047	785
		1.800	0.701	0.88	0.878	0.853	732			0.025	683
		1.297	0.480	0.90	0.896	0.873	858			0.023	784
Average deviation		1.030	0.399	0.90	0.885	0.862	1136			0.023	1042
										1.58%	

$$a_c = \frac{(36S_{ligament} + 24S_{node})}{V_c}$$

$$= \frac{1}{\sqrt{2}L} \left(\frac{3}{2} \alpha \beta (2\pi - 3\Omega) + \frac{45}{32} \pi \alpha^2 (1 - \varepsilon_s) \right), \quad (15)$$

where $S_{ligament}$ and S_{node} are the surface area of one ligament and node contained in the cubic cell, and $V_c (=2V_T)$ is the volume of the cubic cell.

We have presented a non-dimensional curve $\Omega \cdot a_c \cdot L$ with respect to porosities in Fig. 4 (bottom left). From this curve, one can estimate either a_c or L for known total and strut porosities. The dimensionless parameter $\Omega \cdot a_c \cdot L$ increases with an increase in strut porosity, resulting in a lower specific area for a given total porosity. We have also presented a non-dimensional curve relating $\Omega \cdot \alpha \cdot a_c$ to total

porosity in Fig. 4 (bottom right). Using these curves, one can characterize all the geometrical parameters of any hollow strut. The derived correlations presented above allow foams to be tailored according to different specifications. In this way, foams with desired properties can be made to meet the needs of different engineering applications.

2.2. Comparison with experimental data

Data was gathered from experimental measurements performed on alumina, Mullite, OBSiC and SSiC ceramic foams as given by several authors [13,15,16,26]. These are listed in Table 1.

Theoretically, ε_t and ε_o are independent, but in the results shown in Fig. 5 one observes that for existing

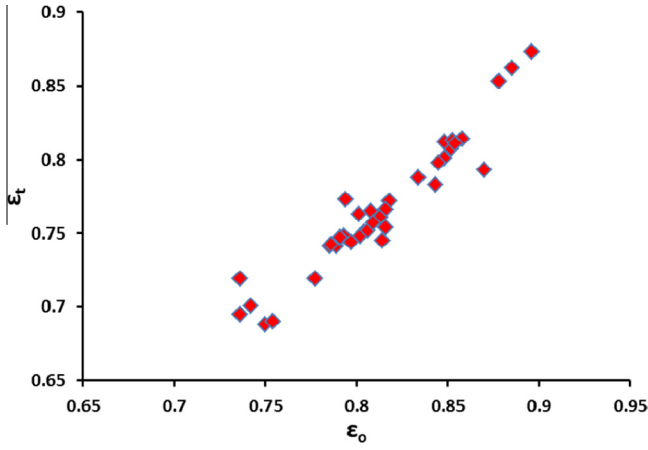


Fig. 5. Relationship between total porosity, ε_t , and open porosity, ε_o , for different material ceramic foams [13,15–16,26].

material foams there is a direct relation between ε_t and ε_o (see also Table 1). This point is used to derive an approximate value of ε_o for a few Mullite and OBSiC ceramic samples that were not measured by Dietrich et al. [15]. Following the general trend of void formation of ceramic foams of different materials, we have determined a fitting relation (see Fig. 5) between ε_t and ε_o which is given by the following equation:

$$\varepsilon_t = 0.9942\varepsilon_o. \quad (16)$$

This fitting relation (Eq. (16)) gives access to calculate the specific surface area analytically for the samples whose open porosities are unknown (see Table 1). We have validated a wide range of specific surface areas measured by different authors [13,15,16,26], and our results are presented in Table 1. The analytical results are in good agreement and the average deviation of 28 different samples of different materials is 1.58%.

It is worth noting that the mathematical correlation is developed for porosity ranging from 65 to 90% for circular strut shapes and triangular voids. Richardson et al. [8] have proposed that for $\varepsilon_t > 0.90$, the strut shape changes from circular to triangular and possesses a circular void. We have presented a mathematical formulation to determine the geometrical properties and specific surface area for porosity $\varepsilon_t > 0.90$ in Appendix A.

3. Pressure-drop correlation in ceramic foams

In the literature, pressure-drop correlations in open-cell foams are often derived via an Ergun-like approach. Recently, Dietrich et al. [15] derived pressure-drop correlations for their ceramic samples and obtained constant numerical values of Ergun parameters as 110 and 1.45, respectively. They calculated the hydraulic diameter using total porosity (ε_t) but not open or hydrodynamic porosity (ε_o). They argued that the two values are closer for their samples and that information about total porosity (ε_t) is more fully available. Permeability is very sensitive to flow conditions and porosity and, in turn, will impact the global pressure drop quite significantly if correct open porosity is not considered [36].

Using the experimental values of flow properties K_1 and K_2 , we compared parameters $A]_D$ and $B]_D$ (calculated using the approach of Dietrich et al. [15], Eq. (3)) and parameters, $A]_E$ and $B]_E$ (calculated using Eq. (2)) and the results are presented in Appendix B (Tables B1 and B2). In Table B1, we observed that the average deviations between parameters $A]_E$ (Eq. (2)) and $A]_D$ (calculated either using hydraulic diameter from pressure-drop measurements or specific surface area) are 35–40%. Similarly, we observed the average deviations between parameters $B]_E$ (Eq. (2)) and $B]_D$ (calculated using either the hydraulic diameter from pressure-drop measurements or the specific surface area) to be 26–28% as presented in Table B2.

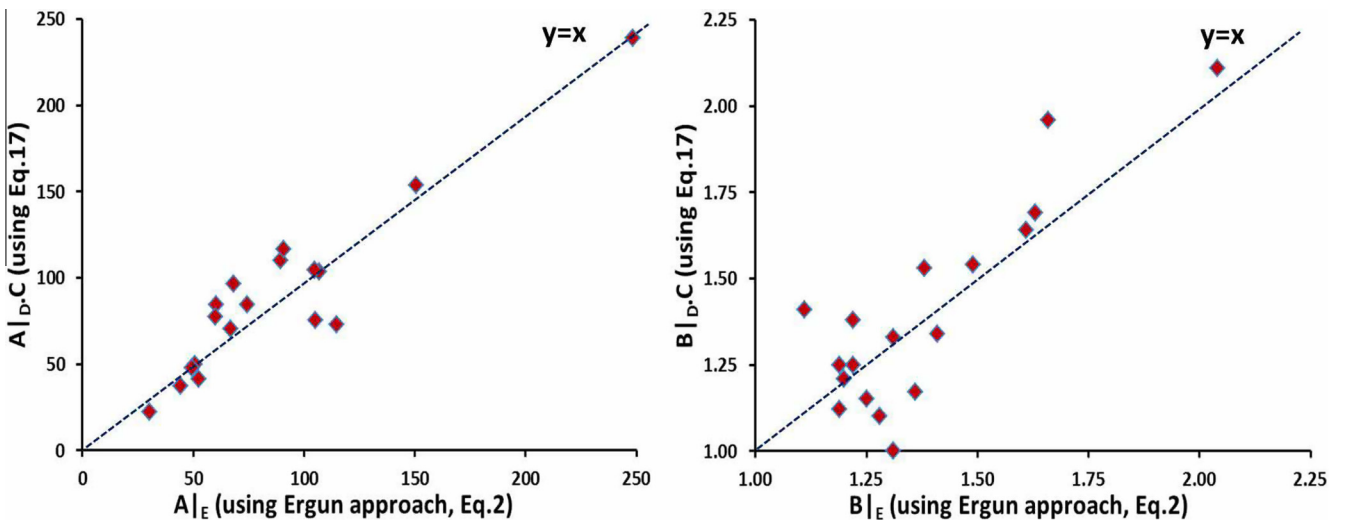


Fig. 6. Left: comparison and validation of Ergun parameter $A]_E$ and $A]_D,C$ Right: comparison and validation of Ergun parameter $B]_E$ and $B]_D,C$.

Table 2

Experimentally and analytically determined flow parameters, K_1 and K_2 of alumina, Mullite and OBSiC ceramic foams of different pore sizes and porosities.

Material	ε_n	Experiments [15]			Analytical		
		$K_1 \times 10^{-9}$ (m ²)	$K_1 \times 10^{-9}$ (m ²) using Eqs. (1) and (2)	$K_1 \times 10^{-9}$ (m ²) using Eqs. (1) and (17)	$K_2 \times 10^{-5}$ (m)	$K_2 \times 10^{-5}$ (m) using Eqs. (1) and (2)	$K_2 \times 10^{-5}$ (m) using Eqs. (1) and (17)
Alumina	0.75	130	116	81	88	83	72
		77	90	108	187	202	225
		54	49	47	114	107	107
	0.80	32	29	28	98	89	91
		20	22	24	76	80	83
		144	180	304	180	201	256
Mullite	0.75	90	71	54	95	85	79
		299	284	274	186	182	184
		88	104	58	122	133	101
	0.80	45	62	43	102	120	102
		29	29	24	66	66	60
		120	129	169	190	197	223
OBSiC	0.75	65	71	56	95	99	95
		276	255	257	135	130	134
		56	54	54	123	120	124
	0.80	46	45	45	84	83	86
		17	11	11	50	41	42
		220	263	379	150	164	193
* Average deviation			2.22%	-2.89%		0.55%	-1.6%

* Average deviation is calculated with respect to experimental values of K_1 and K_2 [15].

These deviations in parameters $A]_D$ and $B]_D$ clearly suggest an inclusion of a correction factor that encompasses the characteristic dimensions of foam structure compared to window or strut diameter or open porosity even if the strut (or inner) porosity is unknown.

We propose to use a correction factor (a dimensionless geometrical parameter) $C = \varepsilon_o(\alpha/\beta)^k$ that needs to be multiplied by $A]_D$ and $B]_D$ to obtain comparable values of $A]_E$ and $B]_E$. The use of factor C will improve the reliability of the correlation and help to reduce the dispersion of calculated values (For α and β , see the analytical approach presented in Section 2.1.).

The relationships between $A]_D$, $B]_D$, $A]_E$ and $B]_E$ are given as follows:

$$\begin{aligned} A]_E &= A]_D \cdot C \text{ and } B]_E \\ &= B]_D \cdot C \text{ with } d_h]_D \text{ from Eq. (3)} \end{aligned} \quad (17)$$

In Fig. 6, we have plotted the relationships presented in Eq. (17) and identify the value of the exponent k that appears in correction factor C . A value of $k = -0.1$ gives the best agreement with the Ergun parameters $A]_E$ and $B]_E$ calculated using Eqs. (2) and (17). However, we could not provide any physical interpretation of the empirical value of k . In order to provide a generic correlation, a systematic study needs to be done.

The average deviations observed for the Ergun parameters $A]_E$ and $B]_E$ obtained from Eqs. (17) and (2) are 7.18% and 0.35%, respectively (see Tables B1 and B2). We have validated the permeability and inertia coefficients

K_1 and K_2 (see Table 2) using the correction factor, C (using Eqs. (1) and (17)). The correlations tend to underestimate the experimental results, the average deviations in calculated properties K_1 and K_2 are -2.89% and -1.6% . One of the reasons for these deviations is the unavailability of experimental values for the specific surface area of a few Mullite foam samples and a complete set of OBSiC foam samples (see Dietrich et al. [15] and Table 1). Note that we extracted a_c using our correlation in Eq. (15) and used this value to carry out all analytical calculations.

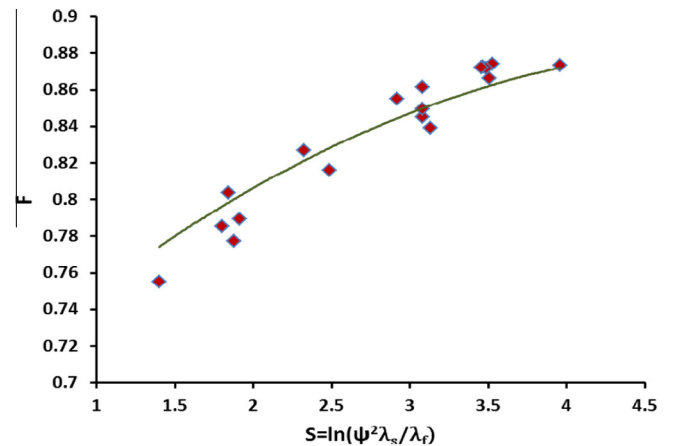


Fig. 7. Plot of F vs. S (non-dimensional).

4. Effective thermal conductivity

4.1. Resistor modeling

We use the resistor modeling approach [45] and apply it to the unit cell in order to incorporate varying individual geometries and non-linear flow of heat flux lines generated by the difference in the thermal conductivity of the constituent phases. The effective thermal conductivity lies between the parallel model and series model of a two-phase system and can be found by incorporating a correlation factor, F . This relationship is given by the following equation:

$$\lambda_{eff} = \lambda_{parallel}^F \cdot \lambda_{series}^{1-F} \quad F \geq 0, 0 \leq F \leq 1, \quad (18)$$

where a F th fraction of the material is oriented in the direction of heat flow and the remaining $(1 - F)$ th fraction is oriented in the perpendicular direction.

The parallel and series models determining conductivity are given by the following:

$$\lambda_{parallel} = \lambda_s(1 - \varepsilon_t) + \varepsilon_t \lambda_f = \psi(\lambda_s - \lambda_f) + \lambda_f, \quad (19)$$

$$\frac{1}{\lambda_{series}} = \left\{ \frac{1 - \varepsilon_t}{\lambda_s} + \frac{\varepsilon_t}{\lambda_f} \right\} = \left\{ \psi \left(\frac{1}{\lambda_s} - \frac{1}{\lambda_f} \right) + \frac{1}{\lambda_f} \right\}, \quad (20)$$

where $\psi = \zeta \alpha^2 \beta (1 - \varepsilon_s) + \Pi \alpha^3 (1 - \Omega \varepsilon_s)$, and ζ and Π are numerical values from Eq. (12).

Eq. (18) is solved for F in terms of, $\lambda_{parallel}$, λ_{series} and λ_{eff} . The solution is given by Eq. (21). Clearly, the factor F contains a geometric function ψ .

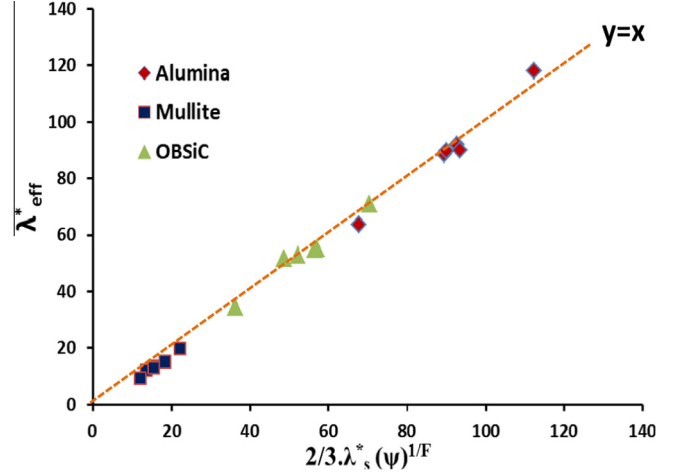


Fig. 8. Plot of λ_{eff}^* vs. $\frac{2}{3} \lambda_s^* (\psi)^{1/F}$ (non-dimensional).

$$F = \frac{\ln \left[(1 - \psi) \frac{\lambda_{eff}}{\lambda_f} + \psi \frac{\lambda_{eff}}{\lambda_s} \right]}{\ln \left[1 + \psi (1 - \psi) \left(\frac{\lambda_s}{\lambda_f} + \frac{\lambda_f}{\lambda_s} - 2 \right) \right]}. \quad (21)$$

For a known ε_t , one can have only one $\lambda_{parallel}$ and λ_{series} which leads to only one value of λ_{eff} for a given value of F . Thus, using this approach implies that the influence of solid matrix geometry (as well as thermophysical properties) will be taken into account only through the F value.

In order to determine a correlation that is more precise than that of Singh and Kasana [45], which is valid for a

Table 3

Experimentally and analytically determined effective thermal conductivity, λ_{eff} of alumina, Mullite and OBSiC ceramic foams of different pore sizes and porosities.

Material	ε_n	Experiments		Analytical			
		λ_{eff}/λ_f	F (*Exp.)	F (*Ana.)	λ_{eff}/λ_f (Using F Ana.)	λ_{eff}/λ_f (Using F Exp.)	λ_{eff}/λ_f (Using F Ana.)
Alumina	0.75	112.39	0.873	0.886	120.15	117.91	120.75
		89.49	0.873	0.872	89.15	88.63	88.48
	0.80	92.79	0.874	0.874	92.53	92.15	92.04
		90.01	0.872	0.872	90.28	89.55	89.67
		93.42	0.882	0.871	88.59	89.96	87.89
		67.67	0.865	0.853	64.03	63.53	61.61
Mullite	0.75	22.01	0.827	0.831	22.29	19.86	20.00
		13.47	0.730	0.813	17.66	12.09	15.02
	0.80	15.48	0.777	0.812	17.29	13.43	14.62
		18.28	0.834	0.810	16.93	15.03	14.22
		15.4	0.785	0.808	16.56	13.05	13.82
		11.94	0.755	0.789	13.26	9.21	10.22
OBSiC	0.75	70.43	0.866	0.873	72.67	70.93	71.81
		52.16	0.841	0.859	56.49	52.70	54.80
	0.80	56.53	0.859	0.859	56.49	54.82	54.80
		57.09	0.862	0.859	56.49	55.08	54.80
		48.52	0.820	0.861	58.11	51.73	56.52
		36.2	0.816	0.837	39.57	34.49	36.54
Average deviation				1.66%	5.04%	5.51%	2.36%

* Exp., experiments; Ana.; analytical.

wider porosity range and solid to fluid thermal conductivity ratios, we used the experimental values provided by Dietrich et al. [46] to support our model. They performed effective thermal conductivity measurements on alumina, Mullite and OBSiC foams for intrinsic solid to fluid thermal conductivity ratios ranging from 140 to 900.

From the λ_{eff} results of Dietrich et al. [46], values of F were extracted using Eq. (21) and a better fit was obtained that includes geometrical parameters and the ratio of constituent phases. We plotted F as function of $S = \ln(\psi^2 \cdot \lambda_s / \lambda_f)$ in Fig. 7. It is observed that F increases, following a roughly quadratic polynomial regime with an increase in S and all the values of factor F for different porosities collapsed on a single curve. There is no physical reason to choose a quadratic polynomial function and we do not claim any physical meaning to the curve fitting. The quadratic polynomial function is the simplest function that gives a good approximation of effective thermal conductivity data. From Fig. 7, it is found that:

$$F = -0.0045^2 + 0.0593S + 0.7144. \quad (22)$$

Due to the scattering of experimental data in Fig. 7, we calculated the root mean square deviation (RMSD) of the fitting relationship in Eq. (22), which is given by following equation:

$$\begin{aligned} RMSD &= 10^{RMS(ELOG)} \text{ with } ELOG \\ &= \log \left(\frac{\lambda_{eff}}{\lambda_f} \right)_{calc} - \log \left(\frac{\lambda_{eff}}{\lambda_f} \right)_{exp}. \end{aligned} \quad (23)$$

We obtained an RMSD value of 0.1088 (or 10.88%) for calculated values of the effective thermal conductivity. From Eq. (22) and Fig. 7, it is evident that F is a function of geometrical parameters and the ratios of the thermal conductivities of constituent phases and is applicable to a wide range of thermal conductivity ratios (λ_s / λ_f).

4.2. Modified Lemlich model

Eq. (4) with an exponent of 1 on solid porosity ($1 - \varepsilon_t$) has been directly used as a check by several authors [39–45]. Thus, there is a need to find an empirical correlation

that incorporates the intrinsic value of the solid thermal conductivity of foams and fluid phase to replace the Lemlich model [38]. In comparison with the resistor model discussed in Section 4.1, we have tried to develop another model based on scattering of the λ_{eff} values of Dietrich et al. [46] that is very similar to the Lemlich model [38].

We propose to use this model [38] by introducing an exponent, n , and replacing the solid porosity ($1 - \varepsilon_t$) by a function of geometrical parameters, ψ . This exponent, n , takes into account the impact of structure on the effective thermal conductivity. We have tried several combinations of λ_{eff} , λ_s , λ_f , ψ and F (from Section 4.1) to find the best fit for all porosities of different materials and intrinsic solid to fluid thermal conductivity ratios ranging from 140 to 900 that collapsed on a single curve. The best fit is presented in Fig. 8. From Fig. 8, the relation is shown to be a straight line given by:

$$\lambda_{eff}^* = \frac{2}{3} \lambda_s^* (\psi)^{1/F}, \quad (24)$$

where $\lambda_{eff}^* = \frac{\lambda_{eff}}{\lambda_f}$ and $\lambda_s^* = \frac{\lambda_s}{\lambda_f}$.

4.3. Validation of resistor and modified Lemlich model

We have validated the effective thermal conductivity results using the resistor model approach and the modified Lemlich model, and this is presented in Table 3. We first compared the correction factor, F that is obtained from the experimental values of Dietrich et al. [46] and Eq. (22). The average deviation observed is 1.66% and suggests that the results of the analytical correlation (Eq. (22)) are a good prediction of F obtained from experiments. Then, we compared the analytical results of λ_{eff} obtained from the resistor model using Eq. (22) and F from experiments. The average deviations are 5.04% and 5.51%, respectively, which establishes that the effective thermal conductivity can be precisely calculated using the resistor model approach if the geometrical parameters or relationship between parameters are known. Lastly, we compared λ_{eff} results obtained from the modified Lemlich model using F obtained from Eq. (22). For this, the average deviation is 2.36%. Thus, all three approaches lead to the same value.

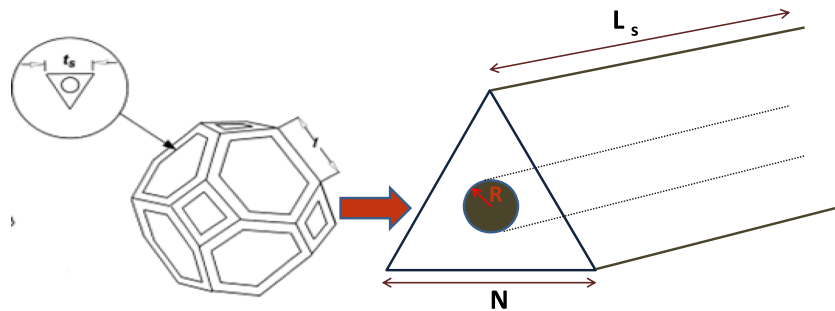


Fig. A1. Left: presentation of a typical hollow ceramic strut with a circular void and triangular strut shape. The image is taken from Ref. [8]. Right: detail of equilateral triangular strut cross-section with circular void inside the strut. The dimensions of strut (side length, N) and void cross-section (void radius, R) are clearly highlighted.

Table B1

Comparison of Ergun parameter, $A]_D$ (pressure drop and specific surface area approach) and $A]_E$ (Ergun approach) of alumina, Mullite and OBSiC ceramic foams.

Material	ε_n	ε_t		ε_t		ε_o	
		Experiments		Calculated		Analytical	
		$d_{h,\Delta P}$ (mm)	d_{h,a_c} (mm)	$A]_D$ [15] using $d_{h,\Delta P}$	$A]_D$ [15] using d_{h,a_c}	$A]_E$ Eq. (2) using Ergun	$A]_E$ Eq. (17) using d_{h,a_c}
Alumina	0.75	3.46	2.75	69.44	43.86	22.13	30.31
		4.1	4.82	176.40	243.79	238.79	248.38
	0.80	2.86	2.66	121.48	105.09	84.19	74.52
		2.34	2.28	137.92	130.93	109.93	89.42
	0.85	1.84	1.7	136.95	116.90	103.49	107
4.24		3.07	106.62	55.89	84.32	60.35	
Mullite	0.75	2.94	2.9	70.69	68.78	37.40	44.34
		4.78	5.01	59.99	65.90	49.95	50.94
	0.80	3.01	3.25	81.23	94.70	41.35	52.51
		2.34	2.77	96.49	135.21	75.26	105.08
	0.85	1.4	1.63	53.87	73.02	47.94	49.48
4.36		3.87	132.12	104.09	116.59	90.97	
OBSiC	0.75	3.22	3.34	118.36	127.35	73.02	114.73
		5.6	5.54	89.88	87.96	70.51	66.83
	0.80	3.33	3.68	156.63	191.29	153.74	150.61
		2.58	2.75	114.46	130.04	104.67	104.92
	0.85	1.86	1.65	159.96	125.88	96.28	68.26
4.18		3.98	67.11	60.84	77.28	59.94	
*Average deviation				40.52%	35.94%		7.18%

* Average deviation is calculated with respect to $A]_E$ of Ergun approach using Eq. (2) considering open porosity.

Table B2

Comparison of Ergun parameter, $B]_D$ (pressure drop and specific surface area approach) and $B]_E$ (Ergun approach) of alumina, Mullite and OBSiC ceramic foams.

Material	ε_n	ε_t		ε_t		ε_o	
		Experiments		Calculated		Analytical	
		$d_{h,\Delta P}$ (mm)	d_{h,a_c} (mm)	$B]_D$ [15] using $d_{h,\Delta P}$	$B]_D$ [15] using d_{h,a_c}	$B]_E$ Eq. (2) using Ergun	$B]_E$ Eq. (17) using d_{h,a_c}
Alumina	0.75	3.46	2.75	2.24	1.78	1.10	1.28
		4.1	4.82	1.43	1.68	1.53	1.38
	0.80	2.86	2.66	1.61	1.50	1.21	1.20
		2.34	2.28	1.55	1.51	1.25	1.22
	0.85	1.84	1.7	1.58	1.46	1.25	1.19
4.24		3.07	1.72	1.24	1.41	1.11	
Mullite	0.75	2.94	2.9	1.68	1.65	1.12	1.19
		4.78	5.01	1.58	1.66	1.33	1.31
	0.80	3.01	3.25	1.54	1.66	1.00	1.31
		2.34	2.77	1.44	1.71	1.17	1.36
	0.85	1.4	1.63	1.35	1.57	1.15	1.25
4.36		3.87	1.60	1.42	1.38	1.22	
OBSiC	0.75	3.22	3.34	1.87	1.94	1.34	1.41
		5.6	5.54	2.60	2.57	2.11	2.04
	0.80	3.33	3.68	1.69	1.87	1.54	1.49
		2.58	2.75	1.92	2.05	1.69	1.63
	0.85	1.86	1.65	2.30	2.04	1.64	1.61
4.18		3.98	1.99	1.89	1.96	1.66	
*Average deviation				28.38%	26.47%		0.35%

* Average deviation is calculated with respect to $B]_E$ of Ergun approach using Eq. (2) considering open porosity.

This signifies the importance of the geometrical parameters of foams on their thermal properties.

The modified Lemlich model validation is presented in Fig. 8. The fit works very well for all known intrinsic λ_s .

We observed an error of $\pm 4\%$ for the entire range of λ_{eff} values, which is comparable to uncertainties in the intrinsic solid-phase conductivity values of Dietrich et al. [46].

5. Conclusion

We have presented a simple mathematical correlation without any fitting curve to characterize ceramic foam geometry. This correlation can be extended to any kind of foam and can be easily applied to different strut shapes with or without voids in struts. The analytical results obtained for the specific surface area have been validated against experimental data of different ceramic foams and are in excellent agreement.

The need for a combination of geometrical parameters has been discussed for flow characteristics and a correction factor C has been suggested to determine Ergun parameters if total porosity is the only known parameter. The new correlation is valid for a large range of porosities and a wide range of Reynolds numbers. All the analytical results of flow properties were validated against experimental results.

Lastly, we derived two effective thermal conductivity models. The first one is based on the resistor approach, while the second one uses the modified Lemlich model. Both models are validated against the experimental values reported in the literature and are found to predict accurately the effective thermal conductivities in the error range of $\pm 5\%$. The final predictions of the analytical models are very effective.

As both models are independent, they can be used simultaneously to predict both the intrinsic solid-phase conductivity (λ_s) and effective thermal conductivity (λ_{eff}) of foams for a known geometry and fluid-phase conductivity. Since the intrinsic solid-phase conductivity is usually unknown, this is extremely useful as it allows the tailoring of foams for many different engineering applications.

Acknowledgements

The authors express their gratitude to ANR (Agence Nationale de la Recherche) for financial support in the framework of FOAM project and all project partners for their assistance.

Appendix A

Mathematical formulation for porosity, $\varepsilon_t > 0.90$:

We have followed the same methodology as presented in Section 2. We have shown a circular void inside an equilateral triangular strut in Fig. A1.

Strut porosity due to void inside the strut is calculated as:

$$\varepsilon_s = \frac{V_{void}}{V_{strut}} = \frac{\pi R^2 L_s}{\sqrt{3}/4 N^2 L_s}. \quad (\text{A.1})$$

Eq. (A.1) can be rewritten as:

$$R = \Omega' N, \quad (\text{A.2})$$

where $\Omega' = \sqrt{\varepsilon_s \sqrt{3}/4\pi}$.

Note that the approximation at the node junction for a triangular strut will be different than for a circular strut cross-section [48], and is given as:

$$0.594N + L_s = L. \quad (\text{A.3})$$

Eq. (A.3) in non-dimension form can be rewritten as:

$$0.594\alpha' + \beta' = 1, \quad (\text{A.4})$$

where $\alpha' = \frac{N}{L}$ and $\beta' = \frac{L_s}{L}$.

Total porosity, ε_s , as a function of geometrical parameters is given by:

$$3\sqrt{3}\alpha'^2\beta'(1 - \varepsilon_s) + \frac{8}{\sqrt{3}}\alpha'^3(1 - \Omega'\varepsilon_s) = 8\sqrt{2}(1 - \varepsilon_t). \quad (\text{A.5})$$

Specific surface area is calculated by the same procedure as derived in Section 2.1 and is given by:

$$a_c = \frac{1}{\sqrt{2}L} \left(\frac{3}{2}\alpha'\beta'(3 - 2\pi\Omega') + \frac{45\sqrt{3}}{128}\alpha'^2(1 - \varepsilon_s) \right) \quad (\text{A.6})$$

Appendix B

Ergun constants $A]_E$ and $B]_E$.
See Tables B1 and B2.

References

- [1] Kim SY, Paek JW, Kang BH. ASME J Heat Transfer 2000;122:572.
- [2] Avenall J. [Master's thesis]. University of Florida, Gainesville, FL;2004.
- [3] Lafdi K, Mesalhy O, Shaikh S. J Appl Phys 2007;102:083549.
- [4] Losito O. PIERS Online 2008;4:805–10.
- [5] Jung A, Natter H, Diebels S, Lach E, Hempelmann R. Adv Eng Mater 2010;13:1527.
- [6] Twigg MV, Richardson JT. Preparation and properties of ceramic foam catalyst supports. In: Poncelet G, Martens J, Delmon B, Jacobs PA, Grange P, editors. Preparation of catalysts VI: studies in surface science and catalysis 91. Amsterdam: Elsevier; 1994. p. 345–59.
- [7] Twigg MV, Richardson JT. Chem Eng Res Des 2002;80:183–9.
- [8] Richardson JT, Peng Y, Remue D. J Appl Catal A 2000;204:19–32.
- [9] Innocentini MDM, Salvini VR, Coury JR, Pandolfelli VC. J Mater Res 1999;4:283–9.
- [10] Reitzmann A, Patcas FC, Kraushaar-Czarnetzki B. Forum Chem Ing Tech 2006;78:885–98.
- [11] Lacroix M, Nguyen P, Schweich D, Huu CP, Savin-Poncet S, Edouard D. Chem Eng Sci 2007;62:3259–67.
- [12] Twigg MV, Richardson JT. Ind Eng Chem Res 2007;46:4166–77.
- [13] Incera Garrido G, Patcas FC, Lang S, Kraushaar-Czarnetzki B. Chem Eng Sci 2008;63:5202–17.
- [14] Huu TT, Lacroix M, Huu CP, Schweich D, Edouard D. Chem Eng Sci 2009;64:5131–42.
- [15] Dietrich B, Schabel W, Kind M, Martin H. Chem Eng Sci 2009;64:3633–40.
- [16] Inayat A, Freund H, Zeiser T, Schwieger W. Chem Eng Sci 2011;66:1179–88.
- [17] Younis L, Viskanta R. Int J Heat Mass Transfer 1993;36:1425–34.
- [18] Lu T, Chen C. Acta Mater 1999;47:1469–85.
- [19] Calmidi VV, Mahajan R. J Heat Transfer 2000;122:557–65.
- [20] Zhao C, Kim T, Lu T, Hodson H. J Thermophys Heat Transfer 2004;18:309–17.
- [21] Giani L, Groppi G, Tronconi E. Ind Eng Chem Res 2005;44:9078–85.

- [22] Scheffler M, Colombo P. Cellular ceramics: structure, manufacturing, properties and applications. New York: Wiley; 2005.
- [23] Snijkers F, Mullens S, Buekenhoudt A, Vandermeulen W, Luyten J. *Mater Sci Forum* 2005;492–493:299–304.
- [24] Gibson LJ, Ashby MF. Cellular solids, structure and properties. 2nd ed. Cambridge: Cambridge University Press; 1999.
- [25] Buciuman FC, Kraushaar-Czarnetzki B. *Ind Eng Chem Res* 2003;42:1863–9.
- [26] Grosse J, Dietrich B, Incera G, Habisreuther P, Zarzalis N, Martin H, et al. *Ind Eng Chem Res* 2009;48:10395–401.
- [27] Vicente J, Topin F, Daurelle JV. *Mater Trans* 2006;47:2195–202.
- [28] Steinhaus H. *Mathematical snapshots*. 3rd ed. New York: Dover; 1999. p. 185–90.
- [29] Wells D. *The penguin dictionary of curious and interesting geometry*. London: Penguin; 1991. p. 232–6.
- [30] Mahjoob S, Vafai K. *Int J Heat Mass Transfer* 2008;51:3701–11.
- [31] Bonnet JP, Topin F, Tadrist L. *Transp Porous Media* 2008;73:233–54.
- [32] Edouard D, Lacroix M, Huu CP, Luck F. *Chem Eng Sci* 2008;144:299–311.
- [33] Ergun S, Orning A. *Ind Eng Chem Res* 1949;41:1179–84.
- [34] Hugo JM, Topin F. *Adv Struct Mater* 2012;13:219–44.
- [35] Dietrich B. *Chem Eng Sci* 2012;74:192–9.
- [36] Inayat A, Schwerdtfeger J, Freund H, Körner C, Singer RF, Schwieger W. *Chem Eng Sci* 2011;66:2758–63.
- [37] Whitaker S. *The method of volume averaging*, vol. 13. Dordrecht: Kluwer; 1999.
- [38] Lemlich RJ. *Colloid Interface Sci* 1978;64:107–10.
- [39] Calmidi VV, Mahajan RL. *J Heat Transfer* 1999;121:466–71.
- [40] Bhattacharya A, Calmidi VV, Mahajan RL. *Int J Heat Mass Transfer* 2002;45:1017–31.
- [41] Fourie JG, Du Plessis JP. *AIChE* 2004;50:547–56.
- [42] Hsu CT, Cheng P, Wong KW. *ASME J Heat Transfer* 1995;117:264–9.
- [43] Ashby MF. *Philos Trans R Soc A* 2006;364:15–30.
- [44] Boomsma K, Poulikakos D. *Int J Heat Mass Transfer* 2001;44:827–36.
- [45] Singh R, Kasana HS. *Appl Therm Eng* 2004;24:1841–9.
- [46] Dietrich B, Schell G, Bucharsky EC, Oberacker R, Hoffmann MJ, Schabel W, et al. *Int J Heat Mass Transfer* 2010;53:198–205.
- [47] Hugo JM. [Ph.D. thesis]. Aix-Marseille University; 2012.
- [48] Kanaun S, Tkachenko O. *Int J Eng Sci* 2008;46:551–71.